Light Scattering by Coherently Driven Lattice Vibrations*

J. A. GIORDMAINE AND W. KAISER†
Bell Telephone Laboratories, Murray Hill, New Jersey
(Received 5 November 1965)

Observations of Raman scattering from intense coherently driven lattice vibrations in calcite are reported. The lattice vibrations ($\bar{\nu}(A_1)=1086$ cm^{-1}) are produced by the stimulated Raman effect, and the scattering is observed with low-intensity monochromatic *probe* sources in the red and ultraviolet. The Raman-scattered light is found to be (1) linear in the probe intensity, (2) monochromatic, (3) highly efficient (~3%), (4) approximately equally intense in the Stokes and anti-Stokes, and (5) emitted at angles in agreement with phase-matching conditions. A coupled-wave theory of the scattering is found to account quantitatively for most of the observations. Possible applications for the technique are suggested.

I. INTRODUCTION

THE generation of stimulated Raman light from liquids[1] and solids[2] is accompanied by intense molecular or lattice vibrations.[3,4] Since the Raman light as well as the exciting laser light are generally highly collimated and monochromatic, the stimulated vibrations have a high degree of spatial and temporal coherence in spite of their strong damping. The availability for the first time of intense and coherent optical phonons has suggested a variety of possible experiments and applications.[4]

Observations of coherently driven lattice vibrations by means of the stimulated Raman-Stokes emission are complicated however by a number of factors, including (1) the simultaneous presence of intense emission at various frequencies separated from the laser frequency by positive and negative integral multiples of the vibrational frequency,[5,6] (2) the crucial role played by details of the laser mode distribution,[7,8] saturation effects, (4) the often complex geometry resulting from the use of focused laser light, (5) quantitative disagreement between calculated and experimentally observed Stokes gain factors[9] and (6) in some cases the accompanying stimulated Brillouin scattering.[10]

Observations of the anti-Stokes emission are at present of limited value as a measure of lattice vibrations since this radiation, which may occur by at least two mechanisms,[11] has complex and relatively poorly understood spectral and angular distributions, both highly sensitive to the laser mode distribution.[5]

This paper reports the experimental observation of coherent lattice vibrations by light scattering, an effect predicted by Garmire, Pandarese, and Townes[4] and further discussed by Tang.[12] In our experiments, coherently driven lattice vibrations were generated in calcite by a conventional giant pulse ruby laser. At the same time the excited region of the crystal was illuminated by a collimated *probe* light of different wavelength, the probe being of sufficiently low intensity as to produce no stimulated Raman scattering. Raman scattering of the probe light was observed and found to have the following properties, in agreement with the theory described below: (1) the scattering intensity is proportional to the probe intensity, (2) the maximum intensities of Stokes and anti-Stokes scattering are approximately equal, (3) the probe scattering efficiency

* Presented at the New York Meeting of American Physical Society, January 1965 [J. A. Giordmaine, Bull. Am. Phys. Soc. **10**, 34 (1965)].

† Present address: Physik-Department der Technischen Hochschule, Munich, Germany.

[1] G. Eckhardt, R. W. Hellwarth, F. J. McClung, S. E. Schwarz, D. Weiner, and E. J. Woodbury, Phys. Rev. Letters **9**, 455 (1962); E. J. Woodbury and W. K. Ng, Proc. IRE **50**, 2367 (1962).

[2] G. Eckhardt, D. P. Bortfeld, and M. Geller, Appl. Phys. Letters **3**, 137 (1963).

[3] The stimulated Raman effect and the scattering results reported in this paper are interpreted in terms of coherently driven lattice vibrations. It should be emphasized that the lattice vibrations, due to their strong damping, have occurred experimentally only in coincidence with laser light and stimulated Raman scattering. As such they represent a highly useful description or interpretation of the interaction of multiple light beams. A general phenomenological theory of the interaction of four coupled light waves (applicable to an arbitrary nonlinear medium) has been formulated by J. Armstrong, N. Bloembergen, J. Ducuing, and P. Pershan, Phys. Rev. **127**, 1918 (1962). It was later shown by N. Bloembergen, Proc. IEEE **51**, 124 (1963), and in *Proceedings of the 3rd International Congress on Quantum Electronics, Paris, 1963* (Columbia University Press, New York, 1964), p. 1501, that the stimulated Raman effect can be considered as a resonance in the nonlinear susceptibilities appearing in the theory. Equations (22)–(25) of the present paper are in fact a special case of Eq. (4.12) of the reference by Armstrong *et al.* From this alternative point of view, the results of stimulated Raman experiments, including those reported in this paper, can be discussed without explicit reference to coherent lattice vibrations. Nevertheless, the latter concept, introduced in Ref. 4, appears to provide a more fruitful description which suggests, as discussed in Ref. 4 and in Sec. V below, a variety of new experiments and techniques not implicit in the four-wave interaction picture of stimulated-Raman phenomena.

[4] E. Garmire, F. Pandarese, and C. H. Townes, Phys. Rev. Letters **11**, 160 (1963).

[5] B. P. Stoicheff, Phys. Letters **7**, 186 (1963).

[6] P. D. Maker and R. W. Terhune, Phys. Rev. **137**, A801 (1965).

[7] N. Bloembergen and Y. R. Shen, Phys. Rev. Letters **13**, 720 (1964).

[8] P. Lallemand and N. Bloembergen, Appl. Phys. Letters **6**, 210, 212 (1965).

[9] F. J. McClung, W. G. Wagner, and D. Weiner, Phys. Rev. Letters **15**, 96 (1965); D. Weiner, S. E. Schwarz, and F. J. McClung, J. Appl. Phys. **36**, 2395 (1965); G. Bret and G. Mayer, in *Physics of Quantum Electronics*, edited by P. L. Kelley *et al.*, (McGraw-Hill Book Company, Inc., New York, 1965), p. 180.

[10] R. Y. Chiao, C. H. Townes, and B. P. Stoicheff, Phys. Rev. Letters **12**, 592 (1964).

[11] E. Garmire, in *Physics of Quantum Electronics*, edited by P. L. Kelley *et al.*, (McGraw-Hill Book Company, Inc., New York, 1965), p. 167.

[12] C. L. Tang, Phys. Rev. **134**, A1166 (1964).

has the same order of magnitude as the laser Stokes scattering efficiency, (4) the scattering directions agree precisely with the requirements of k-vector conservation; in this work full advantage was taken of crystal birefringence in satisfying the k-vector matching conditions. The probe-light technique is believed to be a potentially useful tool in the study of lattice vibrations.

In Sec. II we derive a simplified theory of Raman scattering of the probe light from driven lattice vibrations in terms of coupled waves. Section III describes observations of scattering from stimulated A_1 vibrations of calcite, with the use of a probe light having a frequency substantially different from the laser frequency. Section IV describes the use of a second laser mode as a probe source, and measurements of the dependence of the scattering on probe intensity. In Sec. V some possible applications of the probe technique are described and our results are discussed and summarized.

In this paper the terms *lattice vibrations* and *optical phonons* will be used synonymously to refer to internal and external nonacoustic vibrations of crystal lattices, and as well to the coherently excited molecular vibrations of liquids and gases.

II. THEORY

In this section we derive the coupled wave equations[13] describing scattering of probe light from phonons during the stimulated Raman effect. Solutions of the equations are described which are applicable to the phase-matched scattering experiments described in Secs. III and IV.

1. Polarizability

As a model of the stimulated Raman process for internal lattice vibrations we consider initially a lattice of fixed noninteracting ions, sufficiently dilute as to require no local field corrections. It will be assumed that the linear polarization theory of Placzek[14] is valid. In this approximation, the (anisotropic) electronic polarizability α_{ij} of an individual ion is given by the expansion

$$\alpha_{ij}=(\alpha_0)_{ij}+(\partial\alpha/\partial q)_{ij}q'. \tag{1}$$

In Eq. (1) q' is an operator representing the amplitude of the particular stimulated normal vibrational mode of the ion. The nonstimulated scattering from other modes is ignored. $(\alpha_0)_{ij}$ is the polarizability of a hypothetical rigid ion having its nuclei fixed at their equilibrium positions.

Let $\mathcal{H}'$ represent the contribution to the total Hamiltonian arising from the interaction of the optical electric field $\mathbf{E}$ with the ion. In the electric-dipole approximation

$$\mathcal{H}'=-\mathbf{p}\cdot\mathbf{E}=-q'(\partial\alpha/\partial q)_{ij}E_iE_j\equiv-q'F(r,t) \tag{2}$$

and

$$F(r,t)=(\partial\alpha/\partial q)_{ij}E_iE_j, \tag{3}$$

where $\mathbf{p}$ is the dipole moment associated with the ionic vibration, and F is an effective force. This paper will make use of the summation convention for repeated tensor indices.

The behavior of the expectation value $\langle q'\rangle\equiv q$ is identical to that of a classical harmonic oscillator (1) if the lowest vibrational states are equally spaced and described by harmonic-oscillator wave functions, or (2) if the system can be approximated by a two-level system in which the populations of ground and excited states do not change significantly during the stimulated Raman action. These results are most easily verified by the semiclassical methods of Jaynes and Cummings.[15]

2. Harmonic-Oscillator Approximation

The vibrational Hamiltonian for the single mode of interest is

$$\mathcal{H}_v=\mathcal{H}_0+\mathcal{H}', \tag{4}$$

where $\mathcal{H}_0$ is the unperturbed Hamiltonian of a simple harmonic oscillator of effective mass M', frequency ω_0; $\mathcal{H}'$ is given by Eq. (2). The matrix elements of $\mathcal{H}_0$ are $(\mathcal{H}_0)_{nm}=W_n\delta_{nm}$, where $W_n=(n+\frac{1}{2})\hbar\omega_0$, $n=0,1,2,\cdots$. The nonzero matrix elements $(q')_{nm}$ have the values $(q')_{n,n+1}=(q')_{n+1,n}=(\hbar/2M'\omega_0)^{1/2}(n+1)^{1/2}$. The nonzero matrix elements of $\mathcal{H}_v$ are therefore $(\mathcal{H}_v)_{nn}=W_n$ and $(\mathcal{H}_v)_{n,n+1}=(\mathcal{H}_v)_{n+1,n}=-(\hbar/2M'\omega_0)^{1/2}F(n+1)^{1/2}$. The equation of motion of q' can now be obtained from the Heisenberg equation of motion

$$dq'/dt=-(1/i\hbar)[\mathcal{H}_v,q']. \tag{5}$$

Calculation of d^2q'/dt^2 by repeated application of Eq. (5), followed by evaluation of the expectation value of both sides of the resulting equation, leads to Eq. (6) for the time dependence of the expectation value q.

$$d^2q/dt^2+\omega_0^2q=F/M'. \tag{6}$$

Equation (6) is valid for an ion in an arbitrary quantum vibrational state. For comparison with results below, it is useful to write Eq. (6) as follows, with the aid of the expression for $(q')_{nm}$ above.

$$d^2q/dt^2+\omega_0^2q=(2q_{01}^2\omega_0/\hbar)F. \tag{6'}$$

It follows from Eq. (6) that an ensemble of ideal noninteracting harmonic oscillators can be treated completely classically in calculating the coherent response to the force F, regardless of the temperature, population distribution and changes in population occurring during the excitation.

---

[13] N. Bloembergen, *Nonlinear Optics* (W. A. Benjamin, Inc., New York, 1965).

[14] G. Placzek, in *Handbuch der Radiologie*, edited by E. Marx (Akademische Verlagsgesellschaft, Leipzig, 1934), 2nd ed., Part II, pp. 209–374.

[15] E. T. Jaynes and F. W. Cummings, Proc. IEEE **51**, 89 (1963); see also J. R. Fontana, R. M. Pantell, and R. G. Smith, J. Appl. Phys. **33**, 2085 (1962).

3. Two-Level Approximation

In the case of an anharmonic oscillator the classical description provided by Eq. (6) will still often be useful. As an example, consider the resonant or near-resonant situation in which F has a single-frequency component $\omega_p \approx \omega_0 = (W_1 - W_0)/\hbar$, and in which there are no other transitions degenerate with $0 \rightarrow 1$; then transitions between other pairs of levels can be ignored in first approximation, and the system represented by two levels. The off-diagonal elements of q' connecting the two levels are again labeled $q_{01} = q_{10}$. Application of the above method leads to Eq. (7) for the time dependence of q:

$$d^2q/dt^2 + \omega_0^2 q = (2q_{01}^2\omega_0 F/\hbar)\delta \tag{7}$$

where

$$\delta = a_0 a_0^* - a_1 a_1^* . \tag{8}$$

In Eq. (8) a_0 and a_1 are the amplitudes of the normalized wave functions of ground and excited states, respectively. The quantity δ, summed over the local ions, represents the local population difference between ground and excited states. The time dependence of δ can readily be shown from Schrödinger's equation to be given by

$$\hbar\omega_0(d\delta/dt) = 2F(d\delta/dt) . \tag{9}$$

Equation (9) equates the work performed by F on the vibrating ion to the increase of probability of finding the ion in the excited state 1.

It follows from Eq. (7) that if the population of the excited state beomes equal to that of the ground state, the coupling between the fields and the coherent lattice vibration vanishes. In the case of an inverted population, $\delta < 0$ on the average, and q is driven 180° out of phase. Such a phase reversal would have consequences in the stimulated Raman effect; it would lead to attenuation of the Stokes wave and amplification of an anti-Stokes wave. For a true harmonic oscillator however, such a phase reversal cannot occur and the population can never be distributed so as to amplify the anti-Stokes wave.

In general, when the driving force F is large, Eqs. (7) and (9) must be solved as coupled nonlinear equations. For many stimulated Raman experiments however, including those reported below, negligible $0 \rightarrow 1$ population transfer occurs (Appendix A), and in addition $\omega_0 \gg kT/\hbar$. Under these conditions $\delta \approx a_0 a_0^* \approx 1$, and Eq. (7) becomes

$$d^2q/dt^2 + \omega_0^2 q = (2q_{01}^2\omega_0/\hbar)F , \tag{7'}$$

identical to Eq. (6') for the simple harmonic oscillator.

4. Interaction with Radiation

We need to generalize Eqs. (6) and (7') to describe the vibration of a closely packed lattice, in this case the A_1 internal vibration of calcite consisting of the symmetric planar breathing motion of the $(CO_3)^{2-}$ ions.[16] The noninteracting-ion model is expected to remain a useful approximation since it is known that the A_1 $(CO_3)^{2-}$ vibration frequency is highly insensitive to its host environment.[16] The model does need to be modified to include local field corrections. The macroscopic equations describing interaction of the fields and the lattice can be written as follows[17]:

$$P_i = \alpha_{ij}' q E_j , \tag{10}$$

$$\frac{d^2q}{dt^2} + \Gamma\frac{dq}{dt} + \omega_0^2 q = \frac{\alpha_{ij}'}{M} E_i E_j , \tag{11}$$

$$\nabla\times(\nabla\times\mathbf{E}) + \frac{1}{c^2}\frac{\partial^2\mathbf{D}}{\partial t^2} = -\frac{4\pi}{c^2}\frac{\partial^2\mathbf{P}}{\partial t^2} . \tag{12}$$

In these equations $q = q(\mathbf{r},t)$ is a scalar representing the local average value of $\langle q' \rangle$ for ions in the neighborhood of $\mathbf{r}$. The macroscopic polarization $\mathbf{P}$ in Eqs. (10) and (12) includes only the nonlinear polarization component associated with the variation of q, and plays the role of a driving term in the wave equation (12). The linear polarization only is included in $\mathbf{D}$ in Eq. (12).

According to the model described earlier, the scattering tensor α_{ij}' is equal to $N(\partial\alpha/\partial q)_{ij}$ modified by local field corrections and the effect of Coulomb interactions with neighboring ions, where N is the number of ions/cm³. In the approximation of infinite wavelength phonons, applicable to optical-frequency Raman experiments with infrared inactive phonons, the tensor form of α_{ij}' is determined by the symmetry of the ionic vibrations and the point symmetry of the crystal. For the 1086 cm^{-1} A_1 vibration in calcite, point symmetry D_{3d}, the nonzero coefficients of α_{ij}' are[18] $\alpha_{xx}' = \alpha_{yy}'$, α_{zz}'. According to the measurements of Couture,[19] $\alpha_{zz}'/\alpha_{yy}' = 0.5$.

It is reported in Ref. 19 that in addition α_{xy}' is nonzero, and in fact dependent on the wave vector of the incident and scattered light. (The cross terms α_{xy}' and α_{xz}' are found to be zero as expected.) This breakdown of the selection rules has been attributed[20] to (a) electron wave functions not localized on the individual ion, and (b) long-range Coulomb interactions between vibrating ions. The α_{xy}' term is irrelevant to the experiments described below, and it will be assumed that otherwise α_{ij}' has the tensor form described above.

The damping constant Γ has been introduced phenomenologically. For a Raman line homogeneously broadened by multiphonon processes one predicts a

---

[16] *Landolt-Börnstein Tables*, edited by K. H. Hellwege (Springer-Verlag, Berlin, 1950), 6th ed., Vol. 1, Part 4, pp. 602–609.

[17] The stimulated Raman effect in isotropic media was first described in terms of semiclassical equations of this type by E. Garmire, E. Pandarese, and C. H. Townes, Ref. 4.

[18] R. Loudon, Advan. Phys. **13**, 423 (1964).

[19] L. Couture, Ann. Phys. (Paris) **2**, 5 (1947); **3**, 520 (1948).

[20] O. Theimer, Can. J. Phys. **34**, 312 (1956); Ann. Phys. (Paris) (to be published).

Lorentzian shape, for which the full width at half-intensity $\Delta\omega_L=\Gamma$. The width of the A_1 calcite line at room temperature is[21] 5.5 cm^{-1}, or $\Gamma=1.0\times10^{12}$ sec^{-1}.

The constant M is a normalized density; for the case of negligible local-field correction and ionic interaction M is equal to $N\hbar/(2q_{01}^2\omega_0)$.

5. The Coupled-Mode Equations

We make use of an orthogonal coordinate system in calcite in which x,y,z correspond to the x_1, x_2, and x_3 axes used in Ref. 22. In this notation z is the optic axis and yz is a mirror plane.

Consider an intense laser field propagating in the yz plane with ordinary polarization.

$$\mathbf{E}_1=\hat{x}A_1e^{i(\mathbf{k}_1\cdot\mathbf{r}-\omega_1t)}+\text{c.c.} \tag{13}$$

Attenuation of $\mathbf{E}_1$ due to the stimulated Raman effect and other losses is ignored. Stimulated Raman emission is observed[3,23] having the same polarization and highly collimated in the direction $\mathbf{k}_1$. We approximate this radiation by a plane monochromatic wave

$$\mathbf{E}_{1s}=\hat{x}A_{1s}(\mathbf{r})e^{i(\mathbf{k}_{1s}\cdot\mathbf{r}-\omega_{1s}t)}+\text{c.c.}, \tag{14}$$

with $\omega_{1s}=\omega_1-\omega_0$. Phonons of wave vector $\mathbf{k}_1-\mathbf{k}_{1s}$ are produced and propagate collinearly with the laser beam.[4]

We wish to examine the interaction with these phonons of a collimated probe beam

$$\mathbf{E}_2=\hat{e}_2A_2e^{i(\mathbf{k}_2\cdot\mathbf{r}-\omega_2t)}+\text{c.c.} \tag{15}$$

The polarization $\hat{e}_2$ of the probe beam is left unspecified (although necessarily ordinary or extraordinary), and the frequency ω_2 and wave vector $\mathbf{k}_2$ are in general arbitrary and unrelated to ω_1 and $\mathbf{k}_1$. The attenuation of the probe beam is ignored. Phonons of frequency ω_0 driven by a force proportional to $A_1A_{1s}^*$ modulate $\mathbf{E}_2$ to produce polarization and scattering at frequencies $\omega_{2s}=\omega_2-\omega_0$ and $\omega_{2a}=\omega_2+\omega_0$. Since the important experimental results involve phase-matched scattering occurring under the mutually exclusive conditions $\mathbf{k}_{2a}-\mathbf{k}_2=\mathbf{k}_1-\mathbf{k}_{1s}$ or $\mathbf{k}_2-\mathbf{k}_{2s}=\mathbf{k}_1-\mathbf{k}_{1s}$, it is possible to treat the Stokes and anti-Stokes probe scattering independently. We denote the Stokes and anti-Stokes scattered probe waves as

$$\mathbf{E}_{2s}=\hat{e}_{2s}A_{2s}(\mathbf{r})e^{i(\mathbf{k}_{2s}\cdot\mathbf{r}-\omega_{2s}t)}+\text{c.c.}, \tag{16}$$

and

$$\mathbf{E}_{2a}=\hat{e}_{2a}A_{2a}(\mathbf{r})e^{i(\mathbf{k}_{2a}\cdot\mathbf{r}-\omega_{2a}t)}+\text{c.c.}, \tag{17}$$

respectively.

For Stokes scattering the total field present is

$$\mathbf{E}=\mathbf{E}_1+\mathbf{E}_{1s}+\mathbf{E}_2+\mathbf{E}_{2s}. \tag{18}$$

Substitution of Eq. (13)–(16) into Eq. (11) leads to Eq. (19) for q:

$$q=\frac{2i}{\omega_0M\Gamma}\Big[\alpha'(\omega_1)_{xx}A_1A_{1s}^*e^{i(\Delta\mathbf{k}_1\cdot\mathbf{r}-\omega_0t)} +\boldsymbol{\alpha}'(\omega_2):\hat{e}_2\hat{e}_{2s}A_2A_{2s}^*e^{i(\Delta\mathbf{k}_2\cdot\mathbf{r}-\omega_0t)}+\text{c.c.}\Big]. \tag{19}$$

In Eq. (19) $\Delta\mathbf{k}_1\equiv\mathbf{k}_1-\mathbf{k}_{1s}$, $\Delta\mathbf{k}_2\equiv\mathbf{k}_2-\mathbf{k}_{2s}$. We also define $\Delta\mathbf{k}\equiv\Delta\mathbf{k}_1-\Delta\mathbf{k}_2$, the mismatch for the over-all scattering process. The frequency dependence of $\boldsymbol{\alpha}'$ has been written explicitly in Eq. (19). From Eqs. (10) and (19) the polarization components at frequencies ω_{1s} and ω_{2s} are given by

$$\begin{aligned}\mathbf{P}=-\frac{2i}{\omega_0M\Gamma}\Big\{&\hat{x}[\alpha'(\omega_1)_{xx}]^2A_1A_1^*A_{1s}e^{i(\mathbf{k}_{1s}\cdot\mathbf{r}-\omega_{1s}t)}\\&+\hat{x}\alpha'(\omega_1)_{xx}\boldsymbol{\alpha}'(\omega_2):\hat{e}_2\hat{e}_{2s}A_2^*A_{2s}A_1e^{i[\mathbf{k}_{1s}+\Delta\mathbf{k})\cdot\mathbf{r}-\omega_{1s}t]}\\&+\boldsymbol{\alpha}'(\omega_2)\cdot\hat{e}_2\alpha'(\omega_1)_{xx}A_1^*A_{1s}A_2e^{i[(\mathbf{k}_{2s}-\Delta\mathbf{k})\cdot\mathbf{r}-\omega_{2s}t]}\\&+\boldsymbol{\alpha}'(\omega_2):\hat{e}_2\hat{e}_{2s}\boldsymbol{\alpha}'(\omega_2)\cdot\hat{e}_2A_2^*A_2A_{2s}e^{i(\mathbf{k}_{2s}\cdot\mathbf{r}-\omega_{2s}t)}\Big\}.\end{aligned} \tag{20}$$

To describe the coupling of the polarization waves of Eq. (19) with the fields of the same frequency by means of Eq. (12) it is necessary to take the crystal birefringence into account. Figure 1 shows the refraction of a wave $\mathbf{E}=\hat{e}Ae^{i(\mathbf{k}\cdot\mathbf{r}-\omega t)}$ into a crystal where it interacts with a polarization wave $\mathbf{P}=\hat{p}Pe^{i(\mathbf{k}'\cdot\mathbf{r}-\omega t)}$ of the same frequency. It is shown from the wave equation in Appendix B that the component of ∇A along the ray direction $\hat{s}$ is given by

$$\hat{s}\cdot\nabla A=dA/ds=2\pi i\omega\hat{e}\cdot\hat{p}Pe^{i(\mathbf{k}'-\mathbf{k})\cdot\mathbf{r}}/nc\cos\alpha, \tag{21}$$

where α is the angle between $\mathbf{k}$ and the ray direction $\hat{s}$.[24] If $\mathbf{E}$ is an ordinary wave, $\alpha=0$.

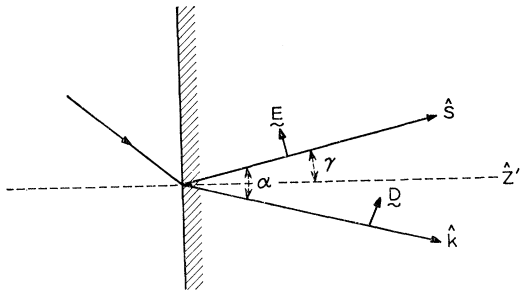

FIG. 1. Refraction of extraordinary probe waves at the surface of a calcite crystal, showing the directions $\hat{k}$ and $\hat{s}$ of the propagation and Poynting vectors, respectively. The unit vector $\hat{z}'$ is normal to the crystal surface. The growth of $\mathbf{E}$ is given in Appendix B and Eq. (21).

[21] R. S. Krishnan, Proc. Indian Acad. Sci. **A22**, 182 (1945).
[22] J. F. Nye, *Physical Properties of Crystals* (Oxford University Press, Oxford, England, 1960), p. 286.
[23] R. Chiao and B. P. Stoicheff, Phys. Rev. Letters **12**, 290 (1964).
[24] An equivalent equation is derived in connection with optical harmonic generation by N. Bloembergen, Ref. 13, pp. 85–88.

The polarization waves of Eq. (18), on substitution into Eq. (19) lead to the coupled wave equations,

$$\begin{aligned} dA_{1s}/ds&=\lambda_{11}|A_1|^2A_{1s}+\lambda_{12}A_2^*A_{2s}A_1e^{i\Delta\mathbf{k}\cdot\mathbf{r}},\\ dA_{2s}/ds&=\lambda_{22}|A_2|^2A_{2s}+\lambda_{21}A_1^*A_{1s}A_2e^{-i\Delta\mathbf{k}\cdot\mathbf{r}}, \end{aligned} \tag{22}$$

where

$$\begin{aligned} \lambda_{11}&=(4\pi\omega_{1s}/n_{1s}cM\Gamma\omega_0)[\alpha'(\omega_1)_{xx}]^2,\\ \lambda_{12}&=(4\pi\omega_{1s}/n_{1s}cM\Gamma\omega_0)\alpha'(\omega_1)_{xx}\boldsymbol{\alpha}'(\omega_2):\hat{e}_2\hat{e}_{2s},\\ \lambda_{21}&=(4\pi\omega_{2s}/n_{2s}cM\Gamma\omega_0\cos\alpha)\alpha'(\omega_1)_{xx}\boldsymbol{\alpha}'(\omega_2):\hat{e}_2\hat{e}_{2s},\\ \lambda_{22}&=(4\pi\omega_{2s}/n_{2s}cM\Gamma\omega_0\cos\alpha)[\boldsymbol{\alpha}'(\omega_2):\hat{e}_2\hat{e}_{2s}]^2. \end{aligned} \tag{23}$$

The ray direction $\hat{s}$ in Eqs. (22) is taken to be common to the laser Stokes and probe Stokes rays. In Eqs. (23) α is the angle between $\hat{s}$ and $\mathbf{k}_{2s}$; n_{1s} and n_{2s} are the refractive indices for laser Stokes and probe Stokes light, respectively.

In the absence of interaction between the probe and laser waves, the second term on the right of each of the coupled wave equations vanishes. The first term can be easily seen to represent the familiar exponential growth of laser Stokes light or probe Stokes light independently. The λ's are real and positive in the resonant case for which $\omega_1-\omega_{1s}=\omega_2-\omega_{2s}=\omega_0$ considered here.

The coupled wave equations for anti-Stokes probe scattering are derived similarly. The total field present is

$$\mathbf{E}=\mathbf{E}_1+\mathbf{E}_{1s}+\mathbf{E}_2+\mathbf{E}_{2a}. \tag{24}$$

From Eqs. (10)–(15), (17), and (21) one obtains the following coupled wave equations for anti-Stokes probe scattering:

$$\begin{aligned} dA_{1s}/ds&=\lambda_{11}'|A_1|^2A_{1s}+\lambda_{12}'A_{2a}^*A_2A_1e^{i\Delta\mathbf{k}\cdot\mathbf{r}},\\ dA_{2a}^*/ds&=-\lambda_{22}'|A_2|^2A_{2a}^*-\lambda_{21}'A_1^*A_{1s}A_2^*e^{-i\Delta\mathbf{k}\cdot\mathbf{r}}. \end{aligned} \tag{25}$$

The λ_{ij}' appearing in Eqs. (25) are identical with the λ_{ij} of Eqs. (23) after the substitution $2s\rightarrow 2a$ is made everywhere in the latter. The angle α is the angle between the propagation direction $\mathbf{k}_{2a}$ and the common ray direction $\hat{s}$.

In the absence of coupling the second terms again vanish; the Eqs. (25) then represent independent exponential growth of laser Stokes and exponential decay of probe anti-Stokes radiation.

6. Probe Stokes Scattering

Solutions of Eqs. (22) for probe Stokes scattering have the form

$$\begin{aligned} A_{1s}&=A_{1s0}e^{(K+i\Delta k/2)s},\\ A_{2s}&=A_{2s0}e^{(K-i\Delta k/2)s}. \end{aligned} \tag{26}$$

We consider only the case of $\Delta\mathbf{k}$ in the ray direction $\hat{s}$. Subsitution in the coupled wave equations leads to a secular equation having solution K_+ and K_- given by

$$\begin{aligned} K_\pm=\tfrac{1}{2}\{&\lambda_{11}|A_1|^2+\lambda_{22}|A_2|^2\\ &\pm[(\lambda_{11}|A_1|^2+\lambda_{22}|A_2|^2)^2-4[(\Delta k/2)^2+i(\Delta k/2)\\ &\times(\lambda_{11}|A_1|^2-\lambda_{22}|A_2|^2)]]^{1/2}\}. \end{aligned} \tag{27}$$

In deriving Eq. (27), use has been made of the exact equality $\lambda_{12}\lambda_{21}=\lambda_{11}\lambda_{22}$.

For phase-matched probe Stokes scattering, the solution representing growing waves is ($\Delta k=0$)

$$K_+=\lambda_{11}|A_1|^2+\lambda_{22}|A_2|^2, \tag{28}$$

for which

$$\frac{A_{2s0}}{A_{1s0}}=\frac{\lambda_{22}A_2}{\lambda_{12}A_1}=\frac{A_2}{A_1}\frac{\omega_{2s}}{\omega_{1s}}\left[\frac{\boldsymbol{\alpha}'(\omega_2):\hat{e}_2\hat{e}_{2s}}{\alpha'(\omega_1)_{xx}}\frac{n_{1s}}{n_{2s}}\right]. \tag{29}$$

Rearrangement of Eq. (29) gives the probe conversion efficiency in terms of the laser conversion efficiency.

$$\frac{|A_{2s}|^2}{|A_2|^2}=\frac{|A_{1s}|^2}{|A_1|^2}\frac{\omega_{2s}^2}{\omega_{1s}^2}\left[\frac{\boldsymbol{\alpha}'(\omega_2):\hat{e}_2\hat{e}_{2s}}{\alpha'(\omega_1)_{xx}}\frac{n_{1s}}{n_{2s}}\right]^2. \tag{30}$$

In our experiments $|A_2|^2\ll|A_1|^2$, implying that the growing wave solution (28)–(30) is predominantly laser Stokes in character, i.e., $|A_{1s}|^2\gg|A_{2s}|^2$.

Equations (28)–(30) show that under phase-matched conditions: (1) the probe Stokes scattering grows exponentially with the same gain as the laser Stokes light. (2) When the probe intensity is small compared to the laser, i.e., $|A_2|^2\ll|A_1|^2$, the gain constant K_+ governing both the laser and the probe Stokes light is negligibly affected by the probe. (3) For arbitrary probe intensity, the gain constant is equal to the sum of the independent gain constants. (4) As long as the probe intensity remains small, the probe scattering efficiency is independent of the probe intensity. The scattering is therefore linear and can be thought of as either Raman scattering or modulation of the probe light by the coherently driven lattice vibrations. (5) The probe scattering efficiency is high, having the same order of magnitude as the conversion efficiency of laser light to laser Stokes light i.e., $|A_{1s}|^2/|A_1|^2$. The above equations and conclusions are valid only for small conversion efficiencies in view of the assumption of negligible depletion of laser and probe sources.

The second and nongrowing solution is ($\Delta k=0$)

$$K_-=0, \tag{31}$$

for which

$$A_{2s0}/A_{1s0}=-(\lambda_{11}A_1^*/\lambda_{12}A_2^*). \tag{32}$$

Since in our experiments $|A_2|^2\ll|A_1|^2$, the nongrowing solution has probe Stokes character, i.e., $|A_{2s}|\gg|A_{1s}|^2$. In experiments in which both A_{1s} and A_{2s} build up together from noise, the nongrowing solution is not observed.

We shall discuss the non-phase-matched case $\Delta k\neq 0$ in

the limit of small probe intensity, i.e., $\lambda_{22}|A_2|^2 \ll \lambda_{11}|A_1|^2$:

$$K_+ \approx \lambda_{11}|A_1|^2+\lambda_{22}|A_2|^2-\frac{i\Delta k}{2} + \frac{i\Delta k\lambda_{22}|A_2|^2}{\lambda_{11}|A_1|^2+\lambda_{22}|A_2|^2-i\Delta k}, \quad (33)$$

$$K_- = \frac{i\Delta k}{2} - \frac{i\Delta k\lambda_{22}|A_2|^2}{\lambda_{11}|A_1|^2+\lambda_{22}|A_2|^2-i\Delta k}. \quad (34)$$

The K_+ solution represents growing waves, the real part of K_+ lying in the narrow range

$$\lambda_{11}|A_1|^2+\lambda_{22}|A_2|^2 \geq K_+ \geq \lambda_{11}|A_1|^2,$$

for all values of Δk. The K_+ solution is always laser Stokes in character. For the K_+ solution,

$$\frac{A_{2s0}}{A_{1s0}} = \frac{\lambda_{22}A_2}{\lambda_{12}A_1}\left(1+\frac{i\Delta k}{\lambda_{11}|A_1|^2+\lambda_{22}|A_2|^2-i\Delta k}\right). \quad (35)$$

On rearrangement on obtains

$$\frac{|A_{2s}|^2}{|A_2|^2} = \left(\frac{1}{f}\right)\frac{|A_{1s}|^2}{|A_1|^2}\frac{\lambda_{22}^2}{\lambda_{12}^2}, \quad (36)$$

where

$$f = 1+\frac{(\Delta k)^2}{(\lambda_{11}|A_1|^2+\lambda_{22}|A_2|^2)^2}. \quad (37)$$

Comparison with Eqs. (30) and (23) shows that when the probe scattering is mismatched by Δk, the probe scattering efficiency decreases by a factor f. The scattering is Lorentzian as a function of Δk, decreasing from the peak value shown in Eq. (30) to half-intensity when $\Delta k = \Delta k_{1/2}$, where

$$\Delta k_{1/2} = \lambda_{11}|A_1|^2+\lambda_{22}|A_2|^2. \quad (38)$$

The half-intensity value of Δk equals the gain constant K_+ at $\Delta k = 0$.

The K_- solution represents, in general, weakly growing waves having probe Stokes character, the real part of K_- lying in the range $\lambda_{22}|A_2|^2 \geq K_- \geq 0$, the maximum and minimum values occurring as $\Delta k \to \infty$ and $\Delta k \to 0$, respectively. In the experiments reported here the probe intensity $|A_2|^2$ was sufficiently low as to produce independently no observable stimulated Raman scattering; it follows that the K_- solution is not directly observed in this work.

In the limit as $\Delta k \to \infty$, K_+ and K_- are exactly the solutions for independent stimulated Raman-Stokes emission by the laser and probe beams, respectively.

7. Probe Anti-Stokes Scattering

The coupled wave Eqs. (25) describing probe anti-Stokes scattering have solutions of the form

$$A_{1s} = A_{1s0}e^{(K'+i\Delta k/2)s}, \qquad A_{2a}^* = A_{2a0}^*e^{(K'-i\Delta k/2)s}. \quad (39)$$

Substitution in Eqs. (25) leads to a secular equation having solutions K_+' and K_-' given by

$$K_\pm' = \tfrac{1}{2}\{\lambda_{11}'|A_1|^2-\lambda_{22}'|A_2|^2 \pm [(\lambda_{11}'|A_1|^2-\lambda_{22}'|A_2|^2)^2-4[(\Delta k/2)^2+i(\Delta k/2) \times(\lambda_{11}'|A_1|^2+\lambda_{22}'|A_2|^2)]]^{1/2}\}. \quad (40)$$

It has again been assumed that $\Delta\mathbf{k}$ is in the ray direction $\hat{s}$.

For phase-matched scattering, the growing-wave solution K_+' is given in Eqs. (41)–(43) ($\Delta k = 0$):

$$K_+' = \lambda_{11}'|A_1|^2-\lambda_{22}'|A_2|^2, \quad (41)$$

and

$$\frac{A_{2a0}^*}{A_{1s0}} = -\frac{\lambda_{22}'A_2^*}{\lambda_{12}'A_1} = -\frac{A_2^*}{A_1^*}\frac{\omega_{2a}}{\omega_{1s}}\left[\frac{\boldsymbol{\alpha}'(\omega_2):\hat{e}_2\hat{e}_{2a}}{\alpha'(\omega_1)_{xx}}\frac{n_{1s}}{n_{2s}}\right], \quad (42)$$

or

$$\frac{|A_{2a}|^2}{|A_2|^2} = \frac{|A_{1s}|^2}{|A_1|^2}\frac{\omega_{2a}^2}{\omega_{1s}^2}\left[\frac{\boldsymbol{\alpha}'(\omega_2):\hat{e}_2\hat{e}_{2a}}{\alpha'(\omega_1)_{xx}}\frac{n_{1s}}{n_{2a}}\right]^2. \quad (43)$$

As in the case of probe Stokes scattering the growing wave has laser Stokes character when $|A_1|^2 \gg |A_2|^2$.

Examination of the anti-Stokes Eqs. (41)–(43) and comparison with the analogous Eqs. (28)–(30) for Stokes scattering lead to the following conclusions: (1) The anti-Stokes probe scattering grows with the same exponential gain as the laser Stokes light. (2) For small probe intensity the laser Stokes gain is unaffected by the probe. (3) For high probe intensity the over-all gain constant is the *difference* of the laser Stokes gain and probe anti-Stokes attenuation, as measured in independent experiments. (4) For low probe intensity, the linear anti-Stokes scattering efficiency $|A_{2a}|^2/|A_2|^2$ should be approximately equal to the Stokes efficiency $|A_{2s}|^2/|A_2|^2$. The ratio of Stokes to anti-Stokes efficiency, from Eqs. (30) and (43), is

$$R = \left(\frac{\omega_{2s}}{\omega_{2a}}\frac{n_{2a}}{n_{2s}}\right)^2 \sim 1. \quad (44)$$

In Eq. (44) it is assumed that any difference in direction between $\hat{e}_{2a}$ and $\hat{e}_{2s}$ can be ignored and that $\alpha'(\omega_2)$ is the same for Stokes and anti-Stokes scattering.

A nongrowing K_-' solution also occurs which, however, is unobservable in our experiments. The behavior of the anti-Stokes scattering as a function of $\Delta\mathbf{k}$ for the case of low probe intensity $\lambda_{22}'|A_2|^2 \ll \lambda_{11}'|A_1|^2$ is analogous to Stokes scattering and need not be repeated. The principal result is that a mismatch of Δk decreases the anti-Stokes scattering efficiency by a factor

$$f' = 1+\frac{(\Delta k)^2}{(\lambda_{11}'|A_1|^2-\lambda_{22}'|A_2|^2)^2}. \quad (45)$$

III. SCATTERING OF ULTRAVIOLET PROBE LIGHT

Observations have been made of angular dependence and efficiency of scattering of ultraviolet probe light from phonons stimulated in calcite by a Q-switched ruby laser. The use of a probe source having a wavelength substantially different from the laser has the advantage of minimizing interaction between the low-intensity-probe experiment and the sometimes extensive tails of the laser-stimulated Stokes and anti-Stokes emission. In our experiments the probe was a coherent source at 3472 Å, derived by harmonic generation[25] in potassium dihydrogen phosphate (KDP) from a portion of the laser beam.

In isotropic media having normal dispersion it is not possible to observe phase-matched ultraviolet probe scattering from the forward phonons induced by the ruby laser (Fig. 2). We have exploited the substantial negative birefringence of calcite to observe these phonons by making use of *ordinary* laser light to generate the phonons and *extraordinary* probe light for the scattering experiment.

The refractive indices of calcite for wavelengths relevant to our experiment were obtained by interpolation of data in Ref. 26, and are shown in Table I. The wave vectors $\mathbf{k}^o(\psi)$ and $\mathbf{k}^e(\psi)$ of ordinary and extraordinary light directed an angle ψ to the optic axis are given by Eqs. (46)[27]:

$$1/(k^o)^2=c^2/\omega^2 n_e^2,$$
$$1/(k^e)^2=(c^2/\omega^2 n_o^2)\cos^2\psi+(c^2/\omega^2 n_e^2)\sin^2\psi. \quad (46)$$

Consider first the collinear scattering experiment of Fig. 3. From Table I and Eq. (46), phase-matched probe Stokes scattering, for which $\Delta k=(k_1-k_{1s})-(k_2-k_{2s})=0$, is calculated to take place at $\psi_s=44°22'$; phase-matched anti-Stokes scattering for which

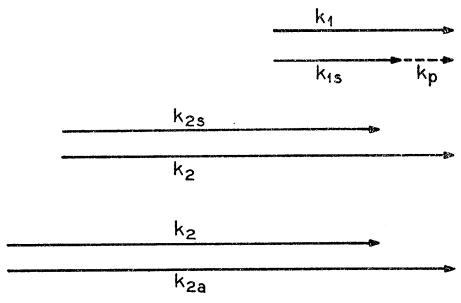

FIG. 2. In an isotropic medium $|\mathbf{k}_2-\mathbf{k}_{2s}|$ and $|\mathbf{k}_{2a}-\mathbf{k}_2|$ exceed $|\mathbf{k}_1-\mathbf{k}_{1s}|$ when the probe frequency ω_2 exceeds the laser frequency ω_1. As a result phase-matched collinear probe scattering is not possible. It is shown in Sec. IV, however, that if $\omega_2\rightarrow\omega_1$ the mismatch becomes negligible.

[25] N. Bloembergen, Ref. 13, Chap. 5.
[26] *International Critical Tables* (McGraw-Hill Book Company, Inc., New York, 1930), Vol. 7, p. 24.
[27] M. Born and E. Wolf, *Principles of Optics* (Pergamon Press, London, 1959), Chap. XIV.

TABLE I. Ordinary and extraordinary refractive index of calcite (18°C) from Ref. 26. The phonon frequency $\omega_0/(2\pi c)=\bar{\nu}(A_1)=1086$ cm^{-1}.

Light	Wavelength (Å)	n_o	n_e
Ruby laser ω_1	6943	1.6526	1.4838
Laser Stokes ω_{1s}	7509	1.6504	1.4828
Probe ω_2	3472	1.6981	1.5045
Probe Stokes ω_{2s}	3608	1.6933	1.5023
Probe anti-Stokes ω_{2a}	3345	1.7033	1.5067

$\Delta k=(k_1-k_{1s})-(k_{2a}-k_2)=0$ occurs at $\psi_a=47°00'$. This experiment is unsatisfactory however, because of the strong double refraction of calcite. For the arrangement of Fig. 3, the extraordinary probe ray can be calculated[27] to deviate from the common direction of the propagation vectors, the laser beam, and the phonons by approximately 7° in the direction remote from the optic axis. For a beam of aperture diameter a, the interaction length is therefore limited to $\sim 8.4\,a$. This effect is closely related to the "aperture effect"[28] limiting the coherence length in optical second-harmonic generation, and will be given the same name below.

Our experiment made use of the geometry shown in Figs. 4 and 5, which results in a reduced aperture effect. For the angles of laser beam and phonon propagation shown, (1) noncollinear Stokes and anti-Stokes scattering occur with $\Delta k=0$, and (2) the probe *ray* travels collinearly with the laser beam and stimulated phonons. Table II contains a summary of the calculated angles (inside the crystal) for phase-matched probe scattering with reduced aperture effect.

These angles were calculated by the following graphical procedure: (1) For a range of angles ψ of laser-beam propagation (the direction of $\mathbf{k}_1$, $\mathbf{k}_{1s}$, and $\mathbf{k}_1-\mathbf{k}_{1s}$), we calculated the angle of incidence of the extraordinary probe wave ω_2 on the laser beam for which the probe *ray* and the laser beam are collinear.[27] (2) From these probe angles the vector $\mathbf{k}_2$ associated with a probe *ray* collinear with the laser beam was calculated as a function of ψ. (3) The vectors $\mathbf{k}_{2s}'\equiv\mathbf{k}_2-(\mathbf{k}_1-\mathbf{k}_{1s})$ and $\mathbf{k}_{2a}'\equiv\mathbf{k}_2+(\mathbf{k}_1-\mathbf{k}_{1s})$ required trigonometrically to close the triangle of Figs. 4 and 5, respectively, were then ob-

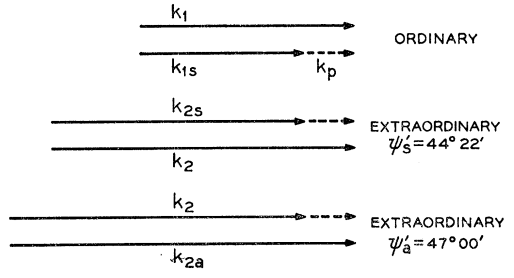

FIG. 3. Collinear phase-matched probe scattering in calcite, with ordinary stimulating laser light and extraordinary probe light. $\bar{\nu}(A_1)=1086$ cm^{-1}.

[28] D. A. Kleinman, Phys. Rev. 128, 1761 (1962), Sec. V.

TABLE II. Beam geometry for phase-matched probe scattering with reduced aperture effect.

	Stokes probe scattering	Anti-Stokes probe scattering
Phonon and laser beam propagation angle, ψ_0	48°41′	50°43′
Probe wave angle of incidence on phonons	6°55′	6°53′
Scattering angle	17′	16′
$\lvert d(\Delta k)/d\psi \rvert$ cm^{-1} deg^{-1}	46	40

tained as a function of ψ. (4) From refractive index data[26] the magnitude k_{2s} (k_{2a}) of the propagation vector of extraordinary light in the *direction* of $\mathbf{k}_{2s}'$ ($\mathbf{k}_{2a}'$) was calculated. (5) The quantity $\Delta k \equiv k_{2s}' - k_{2s}$ ($\Delta k \equiv k_{2a}' - k_{2a}$), a measure of the mismatch in the scattering process, was then plotted *versus* ψ, leading to the values of ψ_0 in Table II for which $\Delta k = 0$. The slope of the graph at $\Delta k = 0$, $d(\Delta k)/d\psi$, will be used below in estimating the angular dependence of the scattering.

The angles of probe wave incidence for phase-matched Stokes and anti-Stokes scattering differ by 2′; since this difference is small compared with experimental uncertainties, the experiment could be set up for both types of scattering with a fixed angle between probe and laser beams. Since the probe ray remains parallel to the laser beam and phonons, the interaction length is determined by the finite widths of the laser, probe, Stokes, and phonon beams, and by the aperture effect due to run-off of the scattered probe light. The 17′ scattering angle of the probe light represents an interaction length of 2×10^2 beam diameters, which for our experiment is greater than the crystal length.

The calcite sample used in this work was cut in the form of a rectangular parallelepiped, with entrance and exit surfaces polished approximately parallel to the (104) cleavage faces. The aperture was 2.5×5.1 cm, and the length was $l = 14.0$ cm. The orientation of the optic axis was found by x-ray measurement on the basis of $d(110) = 2.495$ Å, to be $\zeta = 44°45' \pm 10'$ relative to the end surface normal. For a true (104) face, $\zeta = 44°37'$.

The experimental geometry, based on Table II and $\zeta = 44°45'$ is shown in Fig. 6. Figure 7 shows the apparatus. The Q-switched ruby laser consisted of a 3-in.$\times\frac{3}{8}$ in. ruby, a 90° prism rotating at 10 000 rpm, and a mode-selecting reflector consisting of two uncoated parallel sapphire plates[29]; the over-all cavity length was 40 cm. The laser spectrum consisted of one component, or sometimes two components with a spacing of 2.1 cm^{-1} determined by the mode selector, each component having a spectral width $\sim$0.3 cm^{-1} and consisting of many longitudinal modes of the laser cavity. The laser produced a single pulse of length 20–30 nsec, with polarization normal to Figs. 6 and 7. The average peak laser power in the experiments reported here was 3×10^6 W, with a beam area 0.4 cm^2 and angular divergence 1.6×10^{-3} rad. Approximately 18% of the laser beam was deflected by the 45° glass plate onto the KDP harmonic generator crystal, oriented for light propagation near the phase-matching angle[30] of 50° to the optic axis. Under these conditions a harmonic probe

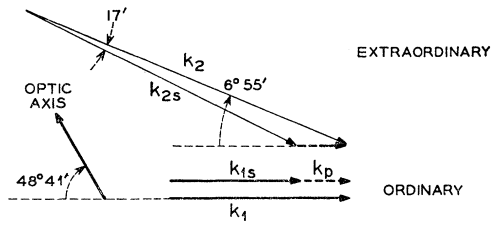

FIG. 4. Noncollinear phase-matched probe Stokes scattering in calcite. At the angles shown the probe *ray* is collinear with $\mathbf{k}_1$, $\mathbf{k}_{1s}$, and $\mathbf{k}_p$.

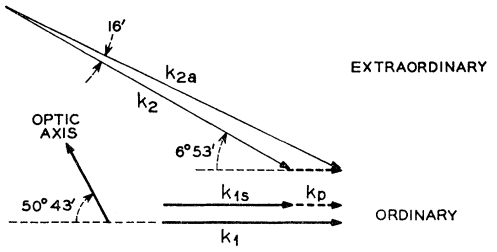

FIG. 5. Noncollinear phase-matched probe anti-Stokes scattering in calcite. The probe *ray* is collinear with $\mathbf{k}_1$, $\mathbf{k}_{1s}$, and $\mathbf{k}_p$.

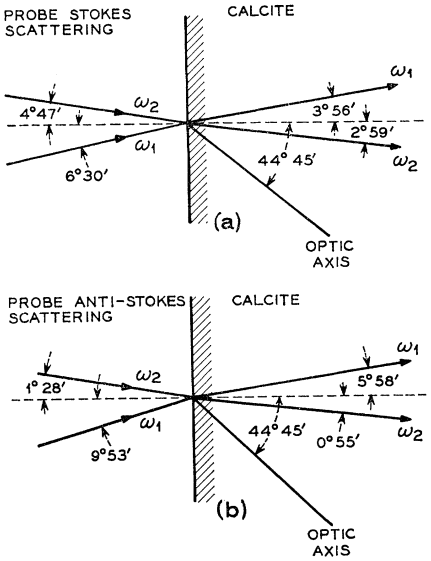

FIG. 6. Calculated geometry of laser (ω_1) and probe (ω_2) beam entry into calcite, for (a) optimum probe Stokes scattering and (b) anti-Stokes scattering.

[29] Laser Systems Center, Ann Arbor, Michigan, Model RR201-66.

[30] J. A. Giordmaine, Phys. Rev. Letters 8, 19 (1962); P. D. Maker, R. W. Terhune, M. Nisenoff, and C. M. Savage, *ibid.* 8, 21 (1962).

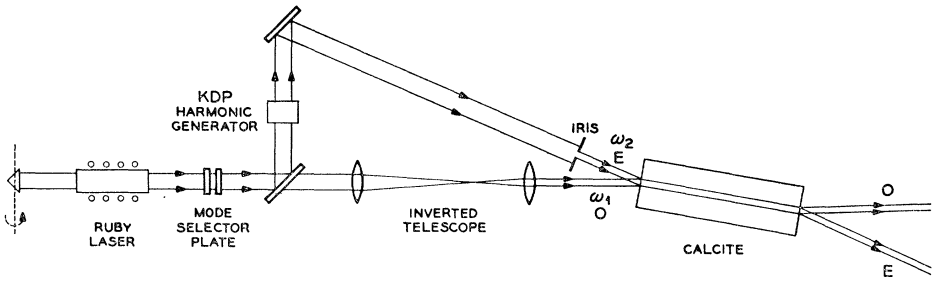

FIG. 7. Probe-scattering apparatus.

power of 500–1000 W was produced, polarized in the plane of Figs. 6 and 7.

With the laser light unfocused, the intensity was indequate to produce stimulated Raman scattering. In preliminary experiments, stimulated Raman scattering, always accompanied by crystal damage, was observed when the laser beam was focused near the center of the crystal with lenses of $f=30$ to 40 cm. The crystal damage usually took the form of a distribution of shatter points distributed at irregular intervals along the beam path. The results of these experiments will be briefly described later.

Most experiments were done with the improved condensing system shown in Fig. 7. The lenses had focal lengths of 30 cm and 10 cm and were separated by 40 cm; this inverted Galilean telescope reduced the beam diameter to about 2.3 mm measured at the calcite crystal, and increased the angular divergence to 5×10^{-3} rad. (17′). The stimulated Raman effect and accompanying probe scattering were observed in this way *without crystal damage.*

The laser and laser Stokes power were measured by deflecting a known fraction of the ordinary transmitted beam onto a diffusely scattering tablet of compressed MgO powder. The scattering properties of such tablets have been found to deviate from Lambert's law by less than 6% for scattering angles less than 60°.[31] The diffused light was detected at a distance of 1–2 m by calibrated 925 phototubes suitably filtered for 6943 and 7509 Å. All measurements of peak intensity were made with an oscilloscope having a nominal rise time of 12 nsec. In the experiments reported here, the average Stokes/laser peak intensity ratio was 12%, with an average deviation of ±4%.

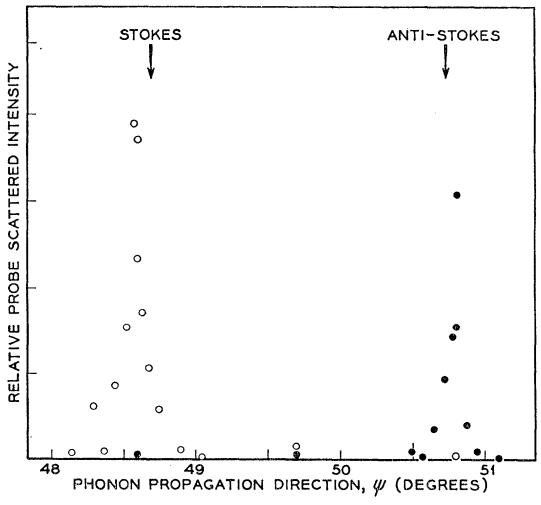

FIG. 8. Probe Stokes and anti-Stokes scattering efficiency as a function of phonon propagation direction ψ. The arrows indicate the calculated angles for phase matched scattering. The open circles represent observations at 3608 Å, the probe Stokes frequency; the closed circles are observations at 3345 Å, the probe anti-Stokes frequency.

The relative intensity of the probe and probe scattered light was measured with the use of a second MgO screen which intercepted the extraordinary beam leaving the crystal. This screen was viewed through a uv transmitting filter by a 935 phototube which measured the probe intensity; a quartz monochromator with 1P28 photomultiplier tube was used to measure probe scattered light diffused from the screen. The monochromator had adequate aperture to detect uv light leaving the crystal within 2° of the probe beam. The 1P28 was calibrated in terms of the 935 probe detector by comparison of the two outputs with the monochromator set for the probe wavelength, 3472 Å. A correction of up to 11% was applied to take into account the variation in relative spectral sensitivity of the detectors over the range 3345 to 3608 Å.

Alignment of the calcite crystal made use of a collimated light beam accurately simulating the laser beam. The crystal was mounted on a precision rotating table with horizontal axis of rotation perpendicular to the laser beam and to the plane of Figs. 6 and 7. To fix the optic axis in a vertical plane, the crystal was first rotated about the beam until the doubly refracted transmitted beams were displaced vertically. With the crystal set near the experimental orientation (Fig. 6) the mirror above the KDP crystal was adjusted to direct the probe beam into the crystal at the same point of entry as the laser beam and at an angle of 11°19′±5′ with the latter. To assure that a large fraction of the transmitted probe light interacted with the phonons, an aperture of diam. 2.9 mm stopped down the probe beam immediately in front of the calcite. A number of tests were made to confirm that the observed probe scattering indeed arose from interaction of laser, laser Stokes, and probe light.

[31] J. A. Giordmaine and K. W. Wecht (unpublished).

It was verified, for example, that probe scattering disappeared (1) when the probe and laser beams traveled through the crystal with a few mm displacement (2) when the laser intensity was reduced slightly to below the stimulated Raman threshold, (3) when the probe beam was blocked.

The probe scattering intensity was measured as a function of the phonon propagation direction angle ψ in the range 48.1° to 51.1°; negligible scattering was observed outside this range. Data were taken with the monochromator set alternately for Stokes and anti-Stokes scattering. Figure 8 is a plot of the results of the longest run. The relative probe-scattered intensity is the ratio (probe-scattered intensity)/(probe intensity), multiplied by a normalization factor to take into account fluctuations from shot to shot of the (laser-Stokes)/(laser) ratio from its average value of 12%. The normalization factor, equal to [(laser intensity)/(laser-Stokes intensity)]×0.12, had a mean deviation from unity of ±30%. Maximum probe Stokes scattering efficiency in Fig. 8 represents an absolute probe scattering efficiency of 3±1%.

The arrows in Fig. 8 show the calculated phonon propagation angles for phase-matched probe scattering (Table II). The measured values of ψ_0 and $\Delta\psi$, the full width of the scattering peak at half-maximum, are shown in Table III.

The estimated value of $\Delta\psi$ is based on the line shape Eqs. (37) and (45), $d(\Delta k)/d\psi$ from Table II, and the following rough estimate of the power gain γ, equal to $2K_+$ (or $2K_+'$) at phase matching. The laser Stokes output is amplified quantum noise, the effective input power to the crystal being zero-point fluctuation noise power $P_i=\epsilon h\nu_{1s}\Delta\nu$ in a band $\Delta\nu$ and a single plane of polarization, where ϵ is the number of spatial modes of the laser beam. For a beam of solid angle $d\Omega$ and area A, $\epsilon=(A/\lambda^2)d\Omega$. For our experiment $\epsilon\approx 10^2$, $\Delta\nu\approx 10^{10}$ sec^{-1}, $h\nu_{1s}=2.65\times10^{-12}$ erg, and $P_i\approx 3$ erg sec^{-1}. The peak output power is $P_0\approx 3\times10^{12}$ erg sec^{-1}. Then $\gamma\approx(1/l)\ln(P_0/P_i)=2.0$ cm^{-1}. Because of the logarithmic dependence of γ on P_i, an order-of-magnitude error in estimating $\Delta\nu$ or ϵ leads to less than 10% error in γ.

From Eqs. (37) and (45) with $\frac{1}{2}\gamma=\lambda_1|A_1|^2\pm\lambda_2|A_2|^2\approx\lambda_1|A_1|^2$, $\Delta k_{1/2}=\gamma/2\approx 1.0$ cm^{-1}, the full width $\Delta\psi$ is estimated from Eq. (47)

$$\Delta\psi=\gamma[d(\Delta k)/d\psi]^{-1}, \tag{47}$$

and leads to the entries in Table III.

TABLE III. Phonon propagation angle ψ_0 and $\Delta\psi$ for maximum probe scattering.

	Stokes probe scattering	Anti-Stokes probe scattering
ψ_0 observed	48°34′	50°47′
ψ_0 calculated	48°41′	50°43′
$\Delta\psi$ observed	5′	3′
$\Delta\psi$ estimated	3′	3′

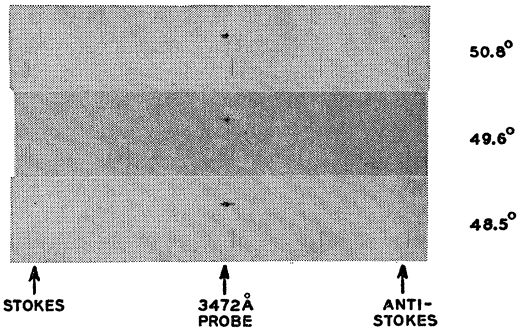

FIG. 9. Spectra of extraordinary probe emission from the calcite crystal for various phonon propagation directions ψ. First-order spectrum, slit width 1 mm=4 Å. The arrows mark the probe Stokes and anti-Stokes wavelengths. The HgCd calibration line spectra were obtained with 10 μ slit. The spectra clearly show the monochromatic Stokes and anti-Stokes probe Raman scattering.

The observed and calculated angles of ψ_0 agree to well within the errors of the calculation and the experiment, each of the order of ±10′. The observed values of $\Delta\psi$ are in order of magnitude agreement with the estimated values; the probe beam width is ~3′ and incapable of resolving finer detail. The shape of the angular distributions of Fig. 8 cannot be fitted to a single Lorentzian curve as suggested by Eqs. (37) and (45); this discrepancy may be caused by nonuniform spatial gain associated with our multimode laser.[8] The observed ratio of Stokes to anti-Stokes scattering, $R\sim 0.8$, is close to one in agreement with Eq. (44).

Of special interest is the result that the probe beam, having an internal width of ~3′, can resolve a peak in the phonon distribution having approximately the same width, and considerably sharper than the exciting laser beam of width ~10′.

The spectrum of the probe scattered light was photographed with low resolving power. For this observation the highly collimated extraordinary transmitted beam was focused onto the spectrograph slit; the slit width was 1 mm, reciprocal linear dispersion 4 Å/mm. Figure 9 shows typical spectra of the probe and probe scattered light in which no extraneous radiation was detected.

High-resolution measurements of the wavelength of the laser and laser Stokes lines with a 2-m spectrograph and Harrison grating, together with the refractive index of air data in Ref. 32, showed the frequency shift of the stimulated Raman Stokes A_1 emission to be 1085.85 ±0.07 cm^{-1}. This result was obtained with an apparent linewidth of laser and laser Stokes light of about 0.4 cm^{-1}. Krishnan[21] finds the A_1 vibration frequency from classical Raman-scattering measurements to be 1085.6 cm^{-1}, with a linewidth of 5.5 cm^{-1}.

In experiments performed prior to those reported above, Stokes and anti-Stokes probe scattering were

[32] *Handbook of Chemistry and Physics*, edited by C. D. Hodgman (Chemical Rubber Publishing Company, Cleveland, 1961), 42nd. ed., p. 2943.

observed in the same calcite sample under different experimental conditions. The laser consisted of a $\frac{1}{4}$-in. diam rod and was Q-switched by a combination of dye and rotating mirror; the peak power was 5 ± 3 MW; the potassium dihydrogen phosphate crystal was in the direct laser beam and provided an order of magnitude greater probe power; the laser and probe beams were *focused* into the calcite crystal with a lens having $f=30$ cm; crystal damage invariably occurred. In this work, the crystal was translated after each laser shot to provide a fresh undamaged track. The results of the experiment were qualitatively consistent with Fig. 8; the peaks occured at $\psi_0=48°15'\pm20'$, $\Delta\psi=24'$ (Stokes) and $\psi_0=50°13'\pm20'$, $\Delta\psi=51'$ (anti-Stokes). The increased width of the scattering peaks is consistent with the $\sim30'$ angular divergence of the focused probe beam, as well as the increased γ at the laser focus. To within the increased experimental uncertainty the observed values of ψ_0 agree with the calculated values (Table III). The measured Stokes to anti-Stokes intensity ratio was $R=0.5$.

Collinear probe scattering (Fig. 3) was also observed with the arrangement described in the above paragraph. In this work, the probe deflection mirrors were adjusted to allow the extraordinary probe beam to enter the crystal parallel to the laser beam, but crossing the latter inside and near the end of the crystal as a result of double refraction. The Raman probe scattering observed in this experiment had a maximum near the expected angles (Fig. 3) but was not otherwise studed in detail. The scattering intensity was much less than in the experiments previously described, since the interaction length was confined to the region of crossing of probe and laser beams.

IV. COLLINEAR PROBE SCATTERING WITHOUT BIREFRINGENCE

Phase-matched probe scattering is most easily observed with a probe frequency ω_2 close to the stimulating laser frequency ω_1. When $\omega_2-\omega_1$ is sufficiently small, phase-matched collinear probe *Stokes* scattering (but not anti-Stokes) can occur in all Raman-active media without the necessity for birefringence (Fig. 1). We have observed this type of scattering in calcite and verified the dependence of scattering intensity on probe intensity predicted in Sec. II. Consider the case of scattering from the A_1 vibration of calcite, where the exciting laser light λ_1 and the collinear probe light λ_2 both have ordinary polarization. For $\lambda_2\approx\lambda_1=6943$ Å, the data of Table I lead to Eq. (48) for the dependence of the mismatch Δk on $\lambda_2-\lambda_1$.

$$\Delta k\equiv(k_1-k_{1s})-(k_2-k_{2s})=9\times10^{-2}(\lambda_2-\lambda_1)\,, \quad (48)$$

where the units of Δk and λ are cm^{-1} and Å, respectively. For a gain at ω_{1s} of $\gamma\sim2$ cm^{-1} it follows from Eqs. (38) and (48) that Δk is negligible if $\lambda_2-\lambda_1 \ll\gamma/(0.09)=22$ Å.

In our experiments the probe source ω_2 consisted of the laser emission in a second weaker emission peak of the mode selector plate described in Sec. III, separated by 2.1 cm^{-1} or 1 Å from the dominant mode, which will be called ω_1 "the laser." For this separation the mismatch Δk is clearly negligible. The intensity distribution between ω_1 and ω_2 could be controlled by variation of the ruby temperature and flash lamp discharge energy. The calcite crystal and other apparatus were arranged as in Fig. 8, except that the uv probe source was removed. Observations were made with laser power about 3×10^6 W and propagation angle $\psi\sim45°$. Both ω_1 and ω_2 sources were ordinary (horizontally polarized), and only the ordinary transmitted component was examined. The transmitted beam was directed onto a ground glass screen several cm from the slit of a high-resolution spectrograph. Figure 10 shows typical spectra of the laser and probe light (left) and the stimulated Raman-Stokes emission and probe-scattered light (right), for several different ratios of probe to laser intensity.

The intensities of the various lines were measured by densitometer on Kodak 1N plates. The plate calibration was established with the aid of a step neutral density filter, calibrated at ω_1 and ω_{1s}, mounted on the slit for all the exposures. Intensity ratios $I(\omega_2)/I(\omega_1)$ and $I(\omega_{2s})/I(\omega_{1s})$ were determined in this way without knowledge of the wavelength dependence of plate sensitivity. All the intensity measurements were based on the peak density at the center of each line. The results for all the plates measured are shown in Fig. 11. The relative probe scattered intensity $I(\omega_{2s})/I(\omega_{1s})=|A_{2s}|^2/|A_{1s}|^2$ is seen to be approximately equal to the relative probe intensity, $I(\omega_2)/I(\omega_1)=|A_2|^2/|A_1|^2$ in the range $0.01<I(\omega_2)/I(\omega_1)<0.3$. This behavior can be accurately compared with the prediction of the s attering theory of Sec. II, Eq. (30), for $\Delta k=0$. In this experiment, $\alpha'(\omega_2):\hat{e}_2\hat{e}_{2s}=\alpha'(\omega_1)_{xx}$, $n_{1s}=n_{2s}$, $\omega_{2s}=\omega_{1s}$,

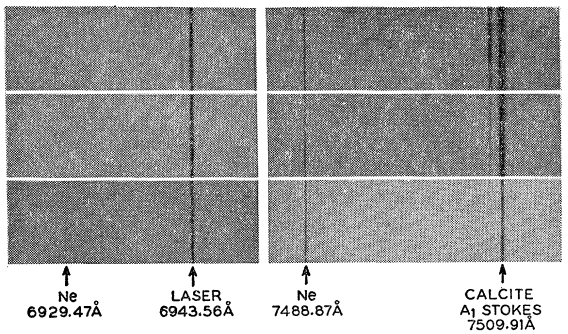

FIG. 10. Spectra of laser with barely visible probe mode (left), and calcite A_1 stimulated Raman Stokes emission with satellite scattering (right). The spectra in each horizontal line were obtained from the same laser shot in different orders of the Harrison grating. The probe intensity increases from bottom to top. The top spectrum shows evidence of weak Raman emission from a third laser mode of lower frequency, not visible at left.

and therefore

$$|A_{2s}|^2/|A_2|^2=|A_{1s}|^2/|A_1|^2. \qquad (30')$$

This predicted behavior is shown by the solid line in Fig. 11 and provides an adequate description of the data.

V. DISCUSSION

In the above experiments the optical probe was found to be a practicable technique in the observation of phonons coherently excited in the stimulated Raman effect. To summarize, the probe scattering was found to have the following properties: (1) Stokes and anti-Stokes scattering efficiencies are equal to or comparable with the efficiency of stimulated Raman emission; (2) the scattering intensity is linear in the probe intensity, as in classical Raman scattering, and the probe

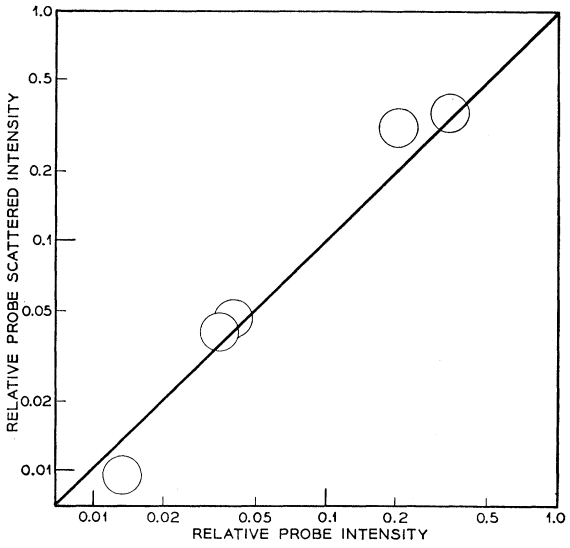

FIG. 11. Relative probe-scattered intensity as a function of relative probe intensity.

can therefore be made sufficiently weak as not to perturb the phonons signficantly; (3) the probe provides information on the angular distribution of phonons with high resolution limited primarily by the angular width of the *probe*. (4) the dependence of scattering efficiency on propagation angles is found to agree with predictions based on **k**-vector matching and on a simple coupled-mode description.

The probe experiment may be compared with other nonlinear Raman experiments involving multiple light beams, in particular the interaction of laser light (ω_1) with Stokes (ω_{1s}) and anti-Stokes (ω_{1a}) light. In calcite, Chiao and Stoicheff[23] report that anti-Stokes emission and Stokes absorption are observed at angles accurately predicted by the matching condition,

$$\Delta\mathbf{k}=(\mathbf{k}_1-\mathbf{k}_{1s})-(\mathbf{k}_{1a}-\mathbf{k}_1)=0. \qquad (49)$$

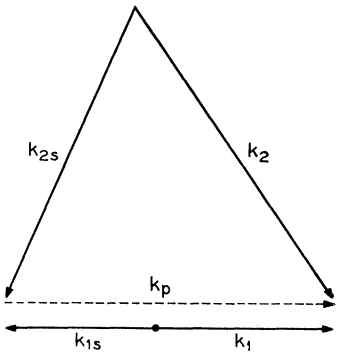

FIG. 12. Possible ultraviolet probe arrangement for observations of phonons associated with *backward*-stimulated Raman scattering.

This behavior is consistent with the description of the stimulated Raman effect given by Garmire, Pandarese, and Townes.[4] Less satisfactory agreement is found in other materials.[5,33] (See, however Ref. 11.) Bloembergen and Shen[34] and others[35] have analyzed in greater detail the same interaction in terms of coupled waves. A striking result of their analyses is that precisely at $\Delta\mathbf{k}=0$, only *nongrowing* solutions occur for both Stokes and anti-Stokes waves. The "dip" or absence of gain at exact phase matching occurs because the gain constant for the coupled waves, analogous to K_+' in Eq. (41), is the sum of a positive (Stokes) component and an equal negative (anti-Stokes) component. The analyses do predict the observed anti-Stokes emission and Stokes absorption close to exact phase matching.

In the probe experiment on the other hand, the $\Delta k=0$ dip is absent both theoretically and experimentally and maximum scattering effects occur at exact phase matching. This simpler behavior occurs for both Stokes and anti-Stokes scattering as long as the probe intensity is small, makes the interpretation relatively straightforward, and undoubtedly contributes to the satisfactory agreement between theory and experiment, even with lasers having substantial spectral and angular width.

The probe technique can be extended to isotropic materials by use of the ruby-laser harmonic[36] as a pump for the stimulated Raman effect, and a small portion of the fundamental as a probe source. The ultraviolet probe technique, applied here in a birefringent material, can in certain cases also be extended to isotropic media. In Fig. 12 for example, phonons having wave vector $\mathbf{k}_1+\mathbf{k}_{1s}$ are produced when $\mathbf{k}_1$ and $\mathbf{k}_{1s}$ are *antiparallel*, and are accessible to uv probe scattering as shown.

Some possible applications of the probe technique are as follows: (1) nonuniform spatial gain[8] as well as other position-dependent properties of the stimulated

[33] See, for example, R. W. Hellwarth *et al.*, Bull. Am. Phys. Soc. **9**, 490 (1964); E. Garmire, *ibid.* **9**, 490 (1964).
[34] N. Bloembergen and Y. R. Shen, Phys. Rev. Letters **12**, 504 (1964); Phys. Rev. **133**, A37 (1964).
[35] See for example, C. L. Tang and T. F. Deutsch, Phys. Rev. **138**, A1 (1965).
[36] R. W. Terhune, P. D. Maker and C. M. Savage, Appl. Phys. Letters **2**, 54 (1963).

Raman action may be analyzed by probe-scattering observations as a function of position along the stimulating laser beam; (2) at low temperatures phonon lifetimes may be sufficiently long in certain materials to permit relaxation measurements on optically stimulated phonons by delayed-probe techniques;[37] (3) optical phonons (ω_1,k_1), (ω_2,k_2) stimulated coherently in an appropriate crystal having an optical (or acoustic) branch near $\omega_1\pm\omega_2$ may induce detectable coherent lattice excitation at $(\omega_1\pm\omega_2,\ k_1\pm k_2)$ as a result of phonon-phonon interactions. The probe technique may be useful in observations of such nonlinear dynamical properties of crystal lattices. (4) Evidence of coherent excitation of "combination phonons" characteristic of both components of a liquid solution has recently been presented.[5,38] Probe experiments would provide more detailed information on the nature of this excitation.

Since the present work was first presented, Brewer[39] has reported observations of nonlinear interaction of hypersonic acoustic waves excited in liquids by stimulated Brillouin scattering. In his work an optical probe at twice the laser frequency was used to observe second-harmonic acoustic waves by collinear Brillouin scattering.

In conclusion, it is of interest to estimate the displacement of the O atoms of the $(CO_3)^{2-}$ ions during the coherent A_1 lattice vibrations observed in these experiments. We denote the root-mean-square displacement by $|\Delta r^2|^{1/2}$. The power per unit volume transferred to the oscillation is $(\omega_0/\omega_{1s})\gamma I_{1s}$, where γ is the Raman Stokes power gain. This power is to be equated to the power dissipated, $\Gamma N(3M_0)\omega_0^2\Delta r^2$, where M_0 is the O atom mass. Corresponding to a maximum Stokes intensity I_{1s} of 10^{14} erg cm^{-2} sec^{-1} and a power gain $\gamma=2$ cm^{-1} one obtains for the O atoms $|\Delta r^2|^{1/2}=2\times10^{-6}$ Å. This value may be compared to a thermal A_1 vibration amplitude of 1×10^{-2} Å at 300°K.

ACKNOWLEDGMENTS

We are indebted to K. W. Wecht for assistance in the experiments, and would like to thank Dr. R. Loudon and Dr. R. C. Miller for a critical reading of the manuscript.

APPENDIX A

The population change $N\Delta\delta$ defined by Eq. (8) occurring during a pulse of stimulated Raman emission is estimated as follows. In the above notation γ represents the power gain per cm for laser Stokes radiation of frequency ω_{1s}, Δt is the pulse duration, and N is the density of vibrating ions. At a position along the beam at which the laser Stokes intensity is I_{1s}, the population change $N\Delta\delta$ is given by

$$\Delta\delta \lesssim 2\gamma I_{1s}\Delta t/N\hbar\omega_{1s}. \tag{A1}$$

This value is an upper limit since relaxation processes have been ignored. In the experiments described in Sec. III, typical values of the parameters in Eq. (A1) are $\gamma=2$ cm^{-1}, $I_{1s}=10^{14}$ erg cm^{-2} sec^{-1}, $\Delta t=3\times10^{-8}$ sec, $N=1.6\times10^{22}$ cm^{-3} and $\hbar\omega_{1s}=2.6\times10^{-12}$ erg. For these values, $\Delta\delta=3\times10^{-4}$. This result indicates that population transfer to the excited state during these experiments can indeed be neglected.

APPENDIX B

Consider a plane wave $\mathbf{E}=\hat{e}Ae^{i(\mathbf{k}\cdot\mathbf{r}-\omega t)}$ propagating in an anisotropic medium (Fig. 1). It is assumed that the amplitude A is a slowly varying function of $\mathbf{r}$ as the result of interaction with a polarization wave $\mathbf{P}=\hat{p}Pe^{i(\mathbf{k}'\cdot\mathbf{r}-\omega t)}$. The vectors $\hat{e}$ and $\hat{p}$ are unit polarization vectors, and $\hat{s}$ and $\hat{k}$ denote the directions of the Poynting and propagation vectors, respectively. We substitute $\mathbf{E}$ and $\mathbf{P}$ into the wave equation (12), making use of the vector relation:

$$\nabla\times(\nabla\times\mathbf{E})=[-A\mathbf{k}\times(\mathbf{k}\times\hat{e})+i\mathbf{k}\times(\nabla A\times\hat{e}) +i\nabla A\times(\mathbf{k}\times\hat{e})]\times e^{i(\mathbf{k}\cdot\mathbf{r}-\omega t)}, \tag{B1}$$

in which second derivatives of A have been ignored, and also the relation:

$$\mathbf{D}=-n^2\hat{k}\times(\hat{k}\times\mathbf{E}). \tag{B2}$$

The substitution leads to:

$$i\mathbf{k}\times(\nabla A\times\hat{e})+i\nabla A\times(\mathbf{k}\times\hat{e}) =(4\pi\omega^2/c^2)P\hat{p}e^{i(\mathbf{k}'-\mathbf{k})\cdot\mathbf{r}}. \tag{B3}$$

The direction of ∇A is that of the surface normal $\hat{z}'$ in Fig. 1, since the surface must be a plane of uniform amplitude. It follows that

$$\nabla A=(\partial A/\partial z')\hat{z}'. \tag{B4}$$

Multiplication of each side of (B3) by $\hat{e}$, and use of (B4), lead to the result

$$-2i\cos\alpha\cos\gamma\frac{n\omega}{c}\frac{\partial A}{\partial z'}=\frac{4\pi\omega^2}{c^2}P\hat{e}\cdot\hat{p}e^{i(\mathbf{k}'-\mathbf{k})\cdot\mathbf{r}}. \tag{B5}$$

The component of ∇A along $\hat{s}$ is therefore

$$\hat{s}\cdot\nabla A=\frac{2\pi i\omega\hat{e}\cdot\hat{p}P}{nc\cos\alpha}e^{i(\mathbf{k}'-\mathbf{k})\cdot\mathbf{r}}. \tag{B6}$$

[37] See for example, N. A. Kurnit, I. D. Abella, and S. R. Hartmann, Phys. Rev. Letters **13**, 567 (1964).
[38] W. Kaiser, M. Maier, and J. A. Giordmaine, Appl. Phys. Letters **6**, 25 (1965).
[39] R. G. Brewer, Appl. Phys. Letters **6**, 165, 230 (1965).

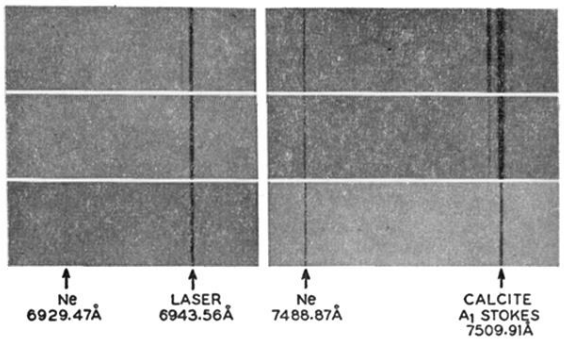

FIG. 10. Spectra of laser with barely visible probe mode (left), and calcite A_1 stimulated Raman Stokes emission with satellite scattering (right). The spectra in each horizontal line were obtained from the same laser shot in different orders of the Harrison grating. The probe intensity increases from bottom to top. The top spectrum shows evidence of weak Raman emission from a third laser mode of lower frequency, not visible at left.

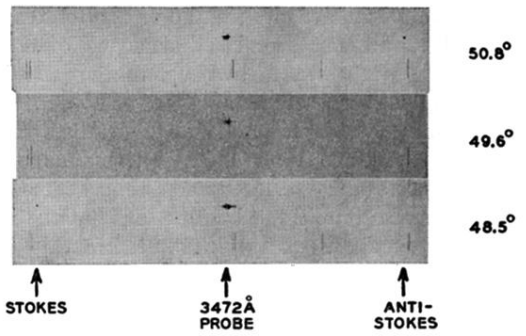

FIG. 9. Spectra of extraordinary probe emission from the calcite crystal for various phonon propagation directions ψ. First-order spectrum, slit width 1 mm=4 Å. The arrows mark the probe Stokes and anti-Stokes wavelengths. The HgCd calibration line spectra were obtained with 10 μ slit. The spectra clearly show the monochromatic Stokes and anti-Stokes probe Raman scattering.